

Limits on variations in fundamental constants from 21-cm and ultraviolet quasar absorption lines

P. Tzanavaris,^{1,*} J. K. Webb,¹ M. T. Murphy,² V. V. Flambaum,¹ and S. J. Curran¹

¹*School of Physics, The University of New South Wales,
Sydney, NSW 2052, Australia*

²*Institute of Astronomy, Madingley Road, Cambridge CB3 0HA, United Kingdom*

(Dated: December 2, 2024)

21-cm and ultraviolet quasar absorption spectra are used to estimate the time variation of $x \equiv \alpha^2 g_p \mu$, where α is the fine structure constant, g_p the proton g factor, and $m_e/m_p \equiv \mu$ the electron/proton mass ratio. The sample used is 8 times larger than previously used. Systematic errors are estimated for the first time. Over a redshift range $0.24 \lesssim z_{\text{abs}} \lesssim 2.04$, $\langle \Delta x/x \rangle_{\text{total}} = (0.35 \pm 1.09) \times 10^{-5}$. A linear fit gives $\dot{x}/x = (-1.30 \pm 1.51) \times 10^{-15} \text{ yr}^{-1}$. Using two previous results on varying α yields the best limits $\Delta \mu/\mu = (1.5 \pm 1.1) \times 10^{-5}$ and $\Delta \mu/\mu = (0.5 \pm 1.1) \times 10^{-5}$.

PACS numbers: 98.80.Es, 06.20.Jr, 95.30.Dr, 95.30.Sf

The existence of extra spatial dimensions, often invoked by superunification theories, may be inferred by the detection of spatial or temporal variations in the value of coupling constants (See [1] for a review). Spectroscopy of gas clouds which intersect the lines of sight to distant quasars is a unique tool, probing the values of these constants over a large fraction of the age of the universe. The highly sensitive many-multiplet method, developed by [2, 3], has been applied on rest-frame ultraviolet (UV) atomic quasar absorption lines to provide constraints on the possible variation of the fine structure constant, $\alpha \equiv e^2/(\hbar c)$ [3, 4, 5, 6]. Molecular hydrogen absorption lines have provided constraints on the variability of the electron-to-proton mass ratio, μ [7, 8, 9].

Principle.— The above results have been obtained by use either of heavy element transitions, which absorb in the rest-frame UV, or of molecular hydrogen transitions. Another approach is to use the parameter $x \equiv \alpha^2 g_p m_e/m_p$ when, apart from rest-frame UV, rest-frame 21-cm absorption, due to cold neutral hydrogen, is also detected. Rest-frame UV absorption is observed redshifted in the optical region, and rest-frame 21-cm is observed redshifted at longer wavelengths of the radio part of the electromagnetic spectrum. The ratio of frequencies $\omega_{21}/\omega_{\text{UV}} \propto x$. 21-cm absorption occurs in a few damped Lyman- α (DLA) systems which also show heavy-element absorption in the UV. A detailed list can be found in [10]. If both UV and 21-cm absorption occur in the same cloud, i.e. at the same physical location, the relative change of the value of x between redshifts z and 0 is related to the observed absorption redshifts for rest-frame 21-cm and UV, z_{21} and z_{UV} , respectively, according to $\Delta x/x \equiv \frac{z_z - x_0}{x_0} = \frac{z_{\text{UV}} - z_{21}}{1 + z_{21}}$ [11]. We obtained values for z_{UV} and z_{21} by using the strongest absorption components in an absorption system. This approach is discussed in detail later.

However, as there are only few such DLAs, there are few results based on this method [11, 12, 13, 14]. Out

of these, only [12] use high-resolution optical data from the Keck telescope's HIRES spectrograph, although they provide an estimate of $\Delta x/x$ at a single redshift from a single absorption system. We applied this method on eight absorption systems from eight quasars covering the redshift range ~ 0.24 to ~ 2.04 . We used all available 21-cm absorption data in conjunction with the highest-resolution UV data available. Thus the results presented here are based on the largest dataset of the highest quality to which this method has been applied to date.

Data analysis.— Details of the 21-cm and UV data used are given in Table I. For the strongest component in each 21-cm absorption complex, the dispersion coordinate, MHz or km s^{-1} , was measured, from which z_{21} was obtained. We searched the optical data for heavy element absorption features close to the redshifts where there is 21-cm absorption. A number of UV absorption features were thus identified, some due to neutral species and most due to singly ionized species. One might expect only the 21-cm and UV *neutral* gases to be spatially coincident (unless the 21-cm gas is primordial or has very low heavy element abundances). However, it was clear in our sample that velocity structure of neutral UV species was followed closely by singly ionized species as well. This means that ionization fraction and abundance do not change significantly along a complex. As shown by [15], this is a general observation for DLAs. This justifies using singly ionized species as well. As neutral species are very rare, one obtains the substantial advantage of a much larger sample. Further, this allowed us to investigate systematics for the first time.

For all UV spectra we determined at which value of the dispersion coordinate, \AA or km s^{-1} , there was strongest absorption in an absorption complex. We then determined absorption redshifts for each detected neutral or singly ionized absorption species that was not saturated. A z_{UV} value was determined individually for each multiplet transition of a single species, e.g. independently

for Zn II 2026.14 and Zn II 2062.66. In all, there were 32 distinct UV species identifications (see Table I, column 6).

Estimating $\Delta x/x$.— Using the relations between $\Delta x/x$, z_{UV} and z_{21} , we obtained a value for $\Delta x/x$ for each $z_{\text{UV}}-z_{21}$ pair. For each heavy element species used in a quasar, we calculated the average $\Delta x/x$ obtained from z_{21} and all z_{UV} values for all transitions of this species. We plot these results in Fig. 1

For each quasar we then calculated the average, $\langle \Delta x/x \rangle_{\text{quasar}}$, of all single $\Delta x/x$ values. This may also be obtained by using corresponding entries for z_{21} and $\langle z_{\text{UV}} \rangle$ in columns 3 and 5 of Table I. Taking the average of all $\langle \Delta x/x \rangle_{\text{quasar}}$ values, we obtained $\langle \Delta x/x \rangle_{\text{total}} = (0.35 \pm 1.09) \times 10^{-5}$ over an absorption redshift range $0.24 \lesssim z_{\text{abs}} \lesssim 2.04$ and a fractional lookback time range $0.20 \lesssim t_{\text{fb}} \lesssim 0.76$, where we have used a Hubble parameter $H_0 = 73 \text{ km s}^{-1} \text{ Mpc}^{-1}$, a total matter density $\Omega_M = 0.27$ and a cosmological constant $\Omega_\Lambda = 0.73$.

The errors quoted are standard deviations on the mean. Alternatively, one might choose to calculate error bars for each system individually, based on the spread of calculated $\Delta x/x$ values for each individual 21-cm/UV pair. However, in reality such errors would be misleading because all UV lines have approximately the same z_{UV} and the error is actually determined by the position of the 21-cm line relative to the UV lines. This error practically does not depend on the spread of the UV transitions.

From these values and the average lookback time, $\langle t_{\text{lb}} \rangle = 6.25 \text{ Gyr}$, we calculate $\langle \Delta x/x \rangle_{\text{total}} / \langle -t_{\text{lb}} \rangle_{\text{total}} = (-0.57 \pm 1.74) \times 10^{-15} \text{ yr}^{-1}$.

For all $z_{\text{UV}}-z_{21}$ values per quasar we calculated the corresponding t_{fb} and the average fractional lookback time per quasar, $\langle t_{\text{fb}} \rangle_{\text{quasar}}$. We then performed a linear least squares fit to $\langle \Delta x/x \rangle_{\text{quasar}} = A \langle t_{\text{fb}} \rangle_{\text{quasar}}$, obtaining $A = (1.73 \pm 2.01) \times 10^{-5}$ [26]. It follows that the rate of change of x as a function of time $\frac{d}{dt}(\Delta x/x) = \dot{x}/x_0 = (-1.30 \pm 1.51) \times 10^{-15} \text{ yr}^{-1}$.

Using strongest components.— Both the 21-cm and UV profiles exhibit complex velocity structure, i.e. have multiple absorption components at slightly different redshifts. That being the case, how does one compare the redshifts among different transitions? As explained, for neutral and singly ionized UV species, velocity structure is essentially the same. This is not the case if one compares 21-cm and UV velocity structure, although we have not systematically searched for corresponding velocity patterns in the 21-cm and UV profiles. One simple option is to measure absorption centroids for each absorption system, which was essentially the approach taken by [12]. Alternatively one can simply determine z_{21} for the strongest component in the 21-cm profile and z_{UV} for the strongest component in each of the UV transitions, and use these. In our sample this is a well defined quantity for both the 21-cm and the UV profiles. Additionally, this procedure should have the advantage of reducing

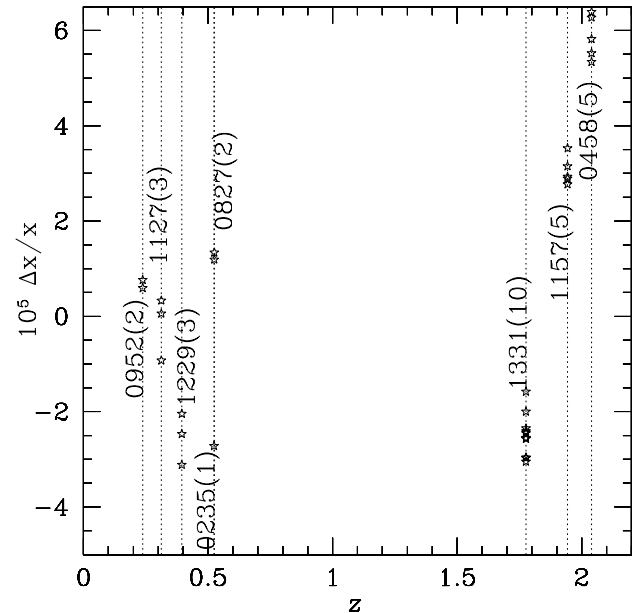


FIG. 1: $\Delta x/x$ results for the eight quasars in our sample. The dotted vertical lines represent z_{21} for each quasar. Quasar names are given truncated to four digits, followed, in brackets, by the number of heavy element species detected. Each point represents average $\Delta x/x$ obtained from z_{21} and z_{UV} , for a single heavy element species in a quasar spectrum, versus average z for that species.

measurement errors caused by broad velocity structure in absorption lines. Nevertheless, the observed redshift difference $z_{\text{UV}} - z_{21}$ between the strongest components of 21-cm and UV may be due to a spatial non-coincidence of hydrogen and heavy elements. For a single absorption complex this is a systematic error. However, for many complexes this error has random sign and magnitude. Therefore, it may be treated as a statistical error when we calculate the mean value of x for many absorption complexes, as we do here.

Discussion of results.— Interestingly, in Fig. 1 it can be seen that there is considerable scatter in the values for $\Delta x/x$. It is evident that for all spectra but Q1127–145, all optically observed species tend to group together in their $\Delta x/x$ values on one side of zero. This is because there is significant offset between, on the one hand, the single z_{21} value and, on the other hand, all z_{UV} values in a system. This suggests that there *is* spatial offset between the 21-cm and UV absorbing gases, but, as expected, this is *random*.

One possible physical explanation for the observed offset may be a large angular size for the emitting 21-cm quasar source, as seen by the absorber. A 21-cm sightline can then intersect a cold, neutral hydrogen cloud with little or no heavy elements, absorbing at z_{21} , whilst a UV/optical sightline can intersect another cloud with

TABLE I: Data used in this work. The results quoted in this paper may be obtained by using corresponding entries in columns 3 and 5. There is one 21-cm/UV absorption system per quasar. Column 1 is the quasar name. Column 2 gives the quasar emission redshift. Column 3 gives the 21-cm absorption redshift for the strongest component. We determined this after digitizing 21-cm absorption plots taken from the references in column 4. The redshift errors introduced in digitizing the data are $\sim 10^{-6}$, more than an order of magnitude smaller than the statistical errors on $\langle z_{\text{UV}} \rangle$ and z_{21} . We do not quote statistical errors on $\langle z_{\text{UV}} \rangle$ and z_{21} since the observed $z_{21} - \langle z_{\text{UV}} \rangle$ is about one order of magnitude larger. Column 5 gives the mean absorption redshift for the strongest UV component closest in redshift to z_{21} . Column 6 gives the UV heavy element species observed in the optical (with number of multiplet transitions in brackets, if more than one). Column 7 gives the source for the UV data. Data for seven quasars were obtained from the European Southern Observatory's (ESO) archive and were originally observed with the UVES spectrograph on the Very Large Telescope (VLT), in which case the ESO program ID is given in column 7 and the principal investigators of the program are given in footnotes. For Q1331+170 we also used a single heavy element absorption plot from Keck/HIRES provided by Art Wolfe. For the eighth quasar (Q0235+164) we digitized an absorption plot from the literature for a single heavy element species.

Quasar	z_{em}	z_{21}	21-cm data	$\langle z_{\text{UV}} \rangle$	ions	UV data
Q0952+179	1.478	0.237804	[16]	0.237812	Mg I, Ca II(2)	69.A-0371(A) ^a
Q1127-145	1.187	0.312656	[17]	0.312651	Ca II(2), Mg I, Mn II(3)	67.A-0567(A) ^b , 69.A-0371(A) ^a
Q1229-021	1.038	0.395004	[18]	0.394969	Ca II(2), Mn II(3), Ti II	68.A-0170(A) ^c
Q0235+164	0.940	0.523874	[19]	0.523833	Mg I	[20]
Q0827+243	0.941	0.524756	[16]	0.524775	Ca II(2), Fe II	68.A-0170(A) ^c , 69.A-0371(A) ^a
Q1331+170	2.097	1.776426	[21]	1.776356	Mg I, Al II, Si II, S II, C I, C I*, Cr II(2), Mn II(2), Fe II(4), Ni II(6), Zn II Si II ^e	67.A-0022(A) ^d , 68.A-0170(A) ^c [21]
Q1157+014	1.986	1.943657	[13]	1.943745	Mg I, Mg II(2), Si II, C II*, Ni II(6)	65.O-0063(B) ^f , 67.A-0078(A) ^f , 68.A-0461(A) ^g
Q0458-0203	2.286	2.039370	[22]	2.039554	Zn II(2), Ni II(6), Mn II(3), Cr II(2), Mg I	66.A-0624(A) ^f , 68.A-0600(A) ^f , 072.A-0346(A) ^f , 074.B-0358(A) ^h

^aSavaglio

^bLane

^cMallén-Ornelas

^dD' Odorico

^eThe same transition as in the UVES data but from Keck/HIRES data.

^fLedoux

^gKanekar

^hDessauges-Zavadsky

heavy elements absorbing at z_{UV} . A large angular size is due to the combined effects of proximity of the absorber to the quasar (small $z_{\text{em}} - \langle z \rangle$) and intrinsic size of radio emitting region.

Comparison with previous results.— [12] used neutral carbon C I, C I*, lines in the Keck/HIRES absorption spectrum of Q1331+170, to obtain $\Delta x/x = (0.70 \pm 0.55) \times 10^{-5}$. For the same object we obtain $\Delta x/x = (-2.5 \pm 3.3) \times 10^{-5}$, the error being the standard deviation of all our $\langle \Delta x/x \rangle_{\text{quasar}}$ values. The value in [12] differs from ours because these authors used a z_{UV} value which is a weighted mean for the observed components [23], thus obtaining a value very close to z_{21} for this absorption system. In our VLT/UVES spectrum of Q1331+170, we detected 23 distinct UV heavy element transitions whose strongest component was well defined within a few km s^{-1} . Further, our use of eight objects allows us to quantify the systematics due to the sightline issues explained above. The error in [12] is exclusively statistical, as it is based on a single absorption system. Although at face value this error is lower than ours, it in-

evitably contains no information on systematics, which, as our error estimate shows, dominate.

A hint for non-zero $\Delta x/x$ from the best objects?—

Q0952+179 is the only quasar for which absorption occurs farthest from the quasar itself and at the lowest redshift for the whole sample. The $\Delta x/x$ value from this spectrum is the closest one to zero. Further, the 21-cm absorption velocity spread in the Q0952+179 21-cm spectrum ($\sim 9 \text{ km s}^{-1}$, full width at half minimum, FWHM) is the smallest amongst all other 21-cm absorption complexes in this sample. Q1229-021, Q0235+164 and Q1331+170 also show small velocity spreads in their 21-cm absorption complexes (~ 10 , ~ 24 and $\sim 24 \text{ km s}^{-1}$, FWHM, respectively). However, only three UV species were used in the case of Q1229-021, the radio spectrum of which is also very noisy. In the case of Q0235+164 only one heavy element transition was used. The spectrum of Q1331+170 has the highest number of UV heavy element absorption features (10 species, 23 transitions). All this suggests that Q1331+170 is the best counterpart of Q0952+179 at high redshift and that

these are the two best objects in our sample. Considering them alone, there is some indication of a smaller x in the past.

Robustness.— We stress that a non-zero $\Delta x/x$ value is not corroborated by the sample as a whole, for which the result is robust. If we use z_{21} from the literature, rather than values determined from our digitized plots, we obtain $\langle \Delta x/x \rangle_{\text{total}} = (0.40 \pm 1.21) \times 10^{-5}$ [27]. If, additionally, we do not use results for Q0235+164, thus excluding any results based on digitized plots, we obtain $\langle \Delta x/x \rangle_{\text{total}} = (0.84 \pm 1.30) \times 10^{-5}$. If we do not use z_{UV} obtained from Ca II, whose ionization potentials are least similar to those for all other elements used here, we obtain $\langle \Delta x/x \rangle_{\text{total}} = (0.41 \pm 1.08) \times 10^{-5}$.

Variation of μ .— Measurements of $x \equiv \alpha^2 g_p m_e / m_p$ are sensitive to variation of several fundamental constants. The proton mass m_p is proportional to the quantum chromodynamic (QCD) scale Λ_{QCD} (defined as the position of the Landau pole in the logarithm for the running strong coupling constant $\alpha_s(r) \sim 1/\ln(\Lambda_{\text{QCD}}r)$). Dependence of the proton mass on the quark mass m_q is very weak ($\Delta m_p/m_p \approx 0.05\Delta m_q/m_q$ [24]) and may be neglected. The dependence of the proton magnetic g factor on the fundamental constants is also quite weak: $\Delta g_p/g_p \approx -0.1 \frac{\Delta(m_q/\Lambda_{\text{QCD}})}{(m_q/\Lambda_{\text{QCD}})}$ [24]. Therefore, the most important effects are due to the variations of α and $\mu \equiv m_e/m_p \approx 0.2m_e/\Lambda_{\text{QCD}}$. From the definition of x one obtains $\frac{\mu_z - \mu_0}{\mu_0} \equiv \Delta\mu/\mu = \Delta x/x - 2\Delta\alpha/\alpha - \Delta g_p/g_p$. Using the $\Delta\alpha/\alpha$ results of [4] and [5], we obtain $\Delta\mu/\mu = (1.5 \pm 1.1) \times 10^{-5}$ and $\Delta\mu/\mu = (0.5 \pm 1.1) \times 10^{-5}$, respectively, assuming $\Delta g_p/g_p \sim 0$. Our result contradicts $\Delta\mu/\mu = (-2.97 \pm 0.74) \times 10^{-5}$ [25] but is consistent with $\Delta\mu/\mu = (0.5 \pm 3.6) \times 10^{-5}$, (2σ) [7]. Note that our result on $\Delta\mu/\mu$ is derived using a completely independent method compared to [7, 25].

Although this is the largest sample used to date, more data are necessary. These may either confirm or reduce the observed scatter, and may also help reduce the gap between $z_{\text{UV}} \sim 0.5$ (Q0827+243) and $z_{\text{UV}} \sim 1.8$ (Q1331+170). More sophisticated analysis, which would involve Voigt profile fitting of absorption features is also possible. However, in virtually all cases, UV components are very clearly coincident in redshift and the result (and its error) is driven by the offset between z_{21} and z_{UV} . Such an analysis would not affect results significantly.

We thank Christian Nutto for help with plot digitization and Art Wolfe for useful discussions and for providing some of the data. This research has made use of the NASA/IPAC Extragalactic Database (NED) which is operated by the Jet Propulsion Laboratory, California Institute of Technology, under contract with the National Aeronautics and Space Administration. Some of the observations were made with ESO telescopes on Paranal.

* Electronic address: pana@phys.unsw.edu.au

- [1] J.-P. Uzan, Rev. Mod. Phys. **75**, 403 (2003).
- [2] V. A. Dzuba, V. V. Flambaum, and J. K. Webb, Phys. Rev. Lett. **82**, 888 (1999).
- [3] J. K. Webb, V. V. Flambaum, C. W. Churchill, M. J. Drinkwater, and J. D. Barrow, Phys. Rev. Lett. **82**, 884 (1999).
- [4] M. T. Murphy, J. K. Webb, and V. V. Flambaum, Mon. Not. R. Astron. Soc. **345**, 609 (2003).
- [5] H. Chand, R. Srianand, P. Petitjean, and B. Aracil, A&A **417**, 853 (2004).
- [6] M. T. Murphy, J. K. Webb, V. V. Flambaum, M. J. Drinkwater, F. Combes, and T. Wiklind, Mon. Not. R. Astron. Soc. **327**, 1244 (2001).
- [7] W. Ubachs and E. Reinhold, Phys. Rev. Lett. **92**, 101302 (2004).
- [8] R. I. Thompson, Astrop. Lett. **16**, 3 (1975).
- [9] C. B. Foltz, F. H. Chaffee, and J. H. Black, Astrophys. J. **324**, 267 (1988).
- [10] S. J. Curran, M. T. Murphy, Y. M. Pihlström, J. K. Webb, and C. R. Purcell (2005), Mon. Not. R. Astron. Soc., accepted, astro-ph/0410647.
- [11] A. D. Tubbs and A. M. Wolfe, Astrophys. J. **236**, L105 (1980).
- [12] L. L. Cowie and A. Songaila, Astrophys. J. **453**, 596 (1995).
- [13] A. M. Wolfe, F. H. Briggs, and D. L. Jauncey, Astrophys. J. **248**, 460 (1981).
- [14] A. M. Wolfe and M. M. Davis, Astron. J. **84**, 699 (1979).
- [15] J. X. Prochaska, Astrophys. J. **582**, 49 (2003).
- [16] N. Kanekar and J. N. Chengalur, A&A **369**, 42 (2001).
- [17] W. Lane, A. Smette, F. Briggs, S. Rao, D. Turnshek, and G. Meylan, Astron. J. **116**, 26 (1998).
- [18] R. L. Brown and R. E. Spencer, Astrophys. J. **230**, L1 (1979).
- [19] A. M. Wolfe, J. J. Broderick, K. J. Johnston, and J. J. Condon, Astrophys. J. **222**, 752 (1978).
- [20] K. M. Lanzetta and D. V. Bowen, Astrophys. J. **391**, 48 (1992).
- [21] A. M. Wolfe, private communication.
- [22] A. M. Wolfe, F. H. Briggs, D. A. Turnshek, M. M. Davis, H. E. Smith, and R. D. Cohen, Astrophys. J. **294**, L67 (1985).
- [23] A. Songaila, L. L. Cowie, S. Vogt, M. Keane, A. M. Wolfe, E. M. Hu, A. L. Oren, D. R. Tytler, and K. M. Lanzetta, Nature **371**, 43 (1994).
- [24] V. V. Flambaum, D. B. Leinweber, A. W. Thomas, and R. D. Young, Phys. Rev. D **69**, 115006 (2004).
- [25] P. Petitjean, A. Ivanchik, R. Srianand, B. Aracil, D. Varshalovich, H. Chand, E. Rodriguez, C. Ledoux, and P. Boissé, Comptes Rendus Acad. Sci. (Paris) **5**, 411 (2004).
- [26] We adopt $\Delta x/x = 0$ at $z = 0$ as the terrestrial value. This has not been checked elsewhere within the Galaxy, and should thus be taken as an assumption.
- [27] For Q0235+164 results based on digitized plots have been used in this calculation as there are no available literature values.